Soils and Foundations 2012;52(4):723–736

The Japanese Geotechnical Society

Soils and Foundations

www.sciencedirect.com
journal homepage: www.elsevier.com/locate/sandf

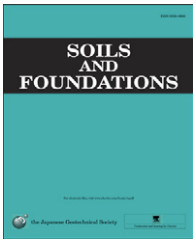

Field axial cyclic loading experiments on piles driven in sand

R J Jardine[a,*], J R Standing[b]

[a]*Professor of Geomechanics, Imperial College London, SW7 2BU, UK*
[b]*Senior Lecturer in Soil Mechanics, Imperial College London, SW7 2BU, UK*

Received 27 November 2011; received in revised form 20 April 2012; accepted 20 June 2012
Available online 11 September 2012

Abstract

Multiple axial cyclic and static loading tests have been performed on industrial steel pipe-piles driven at Dunkerque, northern France. This paper describes the site's geotechnical characteristics and experimental arrangements before defining and describing the stable, unstable or meta-stable responses observed under various combinations of cyclic loading. The interpretation draws on numerical analyses and a parallel model study by Tsuha et al. (2012), relating the field response to the probable shaft shear stress distributions and local effective stress conditions. It is argued that cyclic degradation is controlled by: (i) contraction in the highly constrained interface shear zone and (ii) kinematic yielding within the surrounding soil mass. Finally, interaction diagrams linking shaft response to cyclic loading parameters are proposed based on the field test data and a simplified cyclic capacity predictive approach.

Keywords: Driven piles; Sands; Time; Cyclic loading; Field monitoring

1. Introduction

While axial load cycling can impact significantly on piles, the potential effects are often neglected in design. This paper describes a field investigation into how cyclic loading might affect piles driven in sands. Tsuha et al. (2012) report a related recent laboratory investigation, remarking that influential factors include the number of cycles (N); their frequency (f); the mean load and cyclic amplitude (Q_{mean} and Q_{cyclic}) relative to static capacity Q_{static}; loading history; and the sand characteristics. While their overview of recent developments is not repeated here, we note their comments on the scarcity of field cyclic tests on piles driven in sands and their reference to (i) Lehane's (1992) tests with the 102 mm diameter Imperial College Instrumented Pile (ICP) in Labenne dune sand and (ii) Chow's (1997) ICP experiments and static tests on larger instrumented tubular piles in Dunkerque marine sand.

The limited available data appear to support the cyclic mechanisms proposed by Jardine (1991, 1994).

– While one-way load cycling involves applying cyclic loads of only one sign (tension or compression) to the head of the pile, it is likely, especially at higher load levels, to generate two-way local failure over the upper section of the shaft. The top section of the pile will move more than the soil and apply downward tractions during down-strokes and vice versa. This mechanism promotes top-down progressive cyclic degradation. Stable conditions can be reached if local shaft capacity losses over the upper region can be balanced by load transfer to the toe, or by shaft capacity enhancement at depth (definitions of stable and other states are given later in the paper).

*Corresponding author.
E-mail address: r.jardine@imperial.ac.uk (R. Jardine).
Peer review under responsibility of The Japanese Geotechnical Society.

Production and hosting by Elsevier

0038-0806
http://dx.doi.org/10.1016/j.sandf.2012.07.012

– Two-way cyclic pile loading that involves both compression and tension head loads has the potential to be more damaging than one-way load cycling.
– Local capacity losses result from radial effective stresses reducing in the soil adjacent to the shaft under kinematically controlled conditions, where vertical and circumferential straining is prevented and radial contraction under cyclic shearing is constrained by the (non-linear) stiffness of the soil mass.

Tsuha et al. (2012) report laboratory model tests designed to model these field pile conditions and conclude that shaft capacity can benefit from low-level stable cycling as well as degrade markedly under high-level cycling. In this paper the terms 'low-level' and 'high-level' cycling are used broadly to relate to cyclic load levels that result in an increase or degradation of load capacity compared with the static load capacity. Tsuha et al.'s study also indicates that the influence of prior testing history on cyclic shaft response can be largely accounted for by tracking the changing tension capacities, which they use to normalise the applied cyclic shaft loads.

1.1. Aim and scope of the present study

Full-scale field testing is essential to test the above conjectures. A fully comprehensive study would include a large number of 'fresh' installations to avoid ambiguities relating to any prior testing, but this has yet to be done. The present study employed just seven industrial-scale un-instrumented piles but covered a broad range of Q_{mean} and Q_{cyclic} combinations, as defined in Fig. 1.

The steel pipe-piles (all with 457 mm outer diameter) were driven at a flat part of the Dunkerque Port Ouest Industrial Zone (see Fig. 2); sited about 100 m south of the Institut Pasteur and about 40 m east of the road leading to an oil tank farm. They were installed as part of the GOPAL[1] research project to investigate the potential of forming an enlarged jet-grouted bulb at the base of a driven steel pipe-pile to increase base capacity (see Parker et al., 1999). Two primary piles were installed of the same dimensions: C1, a reference or control pile, and JP1. The latter was a driven steel pile under which a 2.8 m diameter cylindrical jet-grouted base had been formed, but this test is not discussed here. Six additional piles, all approximately 19 m long, were installed to provide reaction for loading the two primary piles, as shown in Fig. 3. Results from the reaction pile predictions and load test measurements indicate that the construction of the jet-grout base had negligible effect on their capacities. Details of the pile wall thicknesses and the precise depths to which they were driven are given in Table 1. The cyclic tests shared facilities with the GOPAL project and were conducted near to the earlier experiments performed on driven steel pipe-piles by the CLAROM[2] group (Brucy et al., 1991; Chow, 1997). Capacity variations with different applied cycling levels were tracked carefully, using conventional instrumentation for field pile testing (details are given by Jardine et al., 2006), to allow load normalisation. The programme of 21 static and 14 cyclic experiments is set out in Table 1. Most testing was performed in tension to simplify the shaft-to-base load split. Numerical modelling was undertaken to evaluate the shaft shear stress distributions and the results are summarised in reports issued to the project sponsors (e.g. Jardine and Standing, 2000). We present here a summary and interpretation of those measurements.

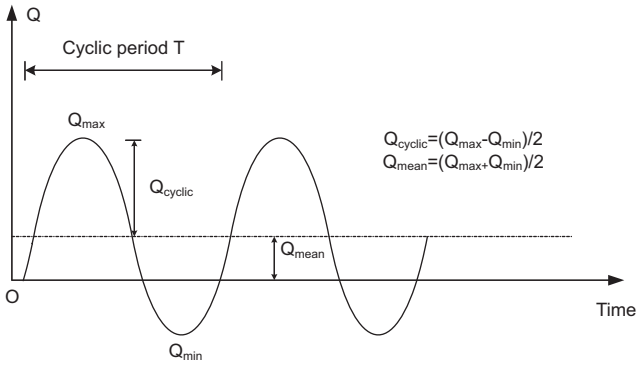

Fig. 1. Schematic illustrating definitions of Q_{mean} and Q_{cyclic} (Tsuha et al., 2012).

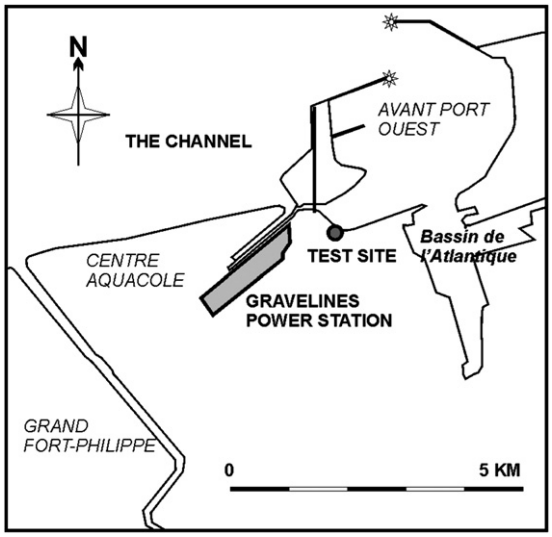

Fig. 2. Location of the test site relative to the Port of Dunkerque (Jardine and Standing, 2000).

1.2. Ground conditions

The site profile consists of 3 m of hydraulic marine sand fill over marine sand. Jardine et al. (2006) describe the

[1]GOPAL is an acronym for Grouted Offshore Piles Alternating Loading.

[2]CLAROM is a French acronym for CLub for Research Activities on Offshore Structures.

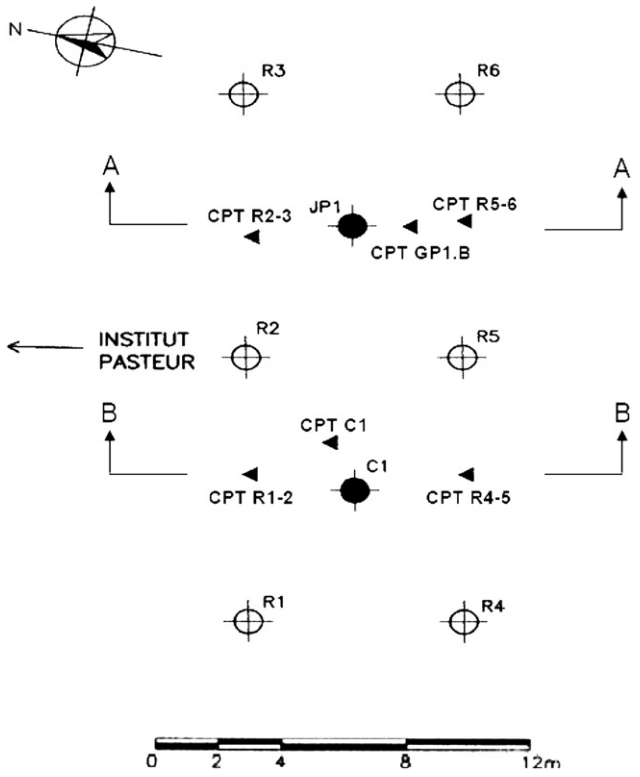

Fig. 3. Plan showing layout of test and reaction piles and CPTs from GOPAL project, Dunkerque (Sections A-A and B-B relate to the CPT profiles shown in Fig. 5).

geology and summarise the site characterisation which included multiple CPT tests, a 26 m sampled borehole, seismic CPT and Marchetti dilatometer profiling, Rayleigh wave testing and laboratory testing. Mineralogical, index, direct and interface shear tests, triaxial stress path, bender element, hollow cylinder torsional shear and resonant column experiments were performed at Imperial College.

The typical site profile is shown in Fig. 4 while Fig. 5 illustrates the local CPT variations and Fig. 6 the particle size distributions. The sub-rounded to rounded grains comprise quartz (84%), albite and microcline (8%) and $CaCO_3$ shell (8%). CPT q_c traces fluctuate with depth and location, typically ranging between 10 and 35MPa. Relative density averages around 75%, but approaches 100% at shallow depth and falls to low values in thin organic layers. Direct shear and triaxial compression tests indicate peak φ' values of 35–40° and critical state values of about 32°, while interface shear tests against steel show design δ values of about 27°. Information is also available regarding elastic anisotropy, non-linear stiffness characteristics and creep behaviour; see Jardine and Standing (2000), Jardine et al. (2005a), (2006), Kuwano (1999) for further details.

1.3. Testing programme

The GOPAL tests applied compression loading to piles C1 and JP1 (see Table 1), bearing against the six reaction piles (R1–R6) as shown in Fig. 3. The minimum pile spacing (s) to diameter (D) ratio was approximately 15. Jardine et al. (2006) report on the driving noting that soil plugs rose to around 60% of the embedded lengths. Three campaigns of load testing took place.

1. August to September 1998—Pile installation and an 'early' static test on R1.
2. October to November 1998—Static testing on C1 and JP1 and both cyclic and static testing on R1, R3, R4, R5 and R6.
3. April 1999—Final static and cyclic testing on all reaction piles; static re-tests on the CLAROM piles.

Table 1 gives pile test codes comprising the: campaign (1–3), pile (e.g. R1), type of test (C=static compression, T=static tension, CY=cyclic) and the number of tests performed up to and including that experiment. The reaction loading for the GOPAL tests was considered to have not affected the reaction piles significantly as none was loaded beyond 60% of its (then current) shaft capacity.

1.4. Effects of local variations in soil conditions on pile capacity

ICP capacity calculations were undertaken to provide an objective assessment of how local geotechnical variations influenced individual pile capacities. These procedures are recognised as providing far better predictive reliability than conventional methods for piles driven in sands and are now applied routinely in offshore geotechnical engineering. Independent database studies by Jardine et al. (2005b) and Lehane et al. (2005) each involving more than 70 high quality pile load tests (typically conducted some days after driving) gave mean ratios of prediction to measurement of 0.95–0.99 and standard deviations around 0.28. As set out by Jardine et al. (2005b), the main steps are as follows.

1. Evaluate the pre-loading shaft radial effective stress distributions from the local CPT tip resistances q_c, the free-field vertical effective stresses σ'_{v0}, P_a the atmospheric pressure and R^* the equivalent radius
   $\sigma'_{rc} = 0.029 q_c (\sigma'_{v0}/P_a)^{0.13} (h/R^*)^{-0.38}$ where
   $R^* = (R^2_{\text{outer}} - R^2_{\text{inner}})^{1/2}$
   h = height above pile tip and $h/R^* \geq 8$

2. The local maximum shaft shear stresses τ_f expected at any given depth on the shaft, and height h above the pile tip are
   $\tau_f = (\sigma'_{rc} + \Delta\sigma'_r)\tan\delta_f$ in compression and
   $\tau_f = 0.9(0.8\sigma'_{rc} + \Delta\sigma'_r)\tan\delta_f$ in tension

3. Where the dilatant component of σ'_r change is
   $\Delta\sigma'_r = 2G\Delta r/R_{\text{outer}}$

Table 1
Summary of pile histories and test codes.

Pile	Pile make up	Testing history	Test Code
R1	20 mm wall thickness	Tension failure 02/09/98	1.R1.T1
Tip at	Over top 2.5 m,	Tension failure 28/10/98	2.R1.T2
19.32 m	13.5 mm to base	Reaction for GOPAL pile tests 02/11 to 06/11/98	–
	Driven 24/08/98	Tension failure 26/04/99	3.R1.T3
R2	As above	Reaction for GOPAL pile tests 29/10 to 6/11/98	–
Tip at	Driven 21/08/98	Tension failure 18/04/99	3.R2.T1
18.85m		Cyclic tension test 18/04/99	3.R2.CY2
		'Quick' static tension failure 18/04/99	3.R2.T3
R3	As above	Reaction for GOPAL pile tests 29/10 to 30/10/98	–
Tip at	Driven 20/08/98	Tension to 2MN—no failure 13/11/98	2.R3.T1
19.24 m		Two sets cyclic tension tests 14 to 15/11/98	2.R3.CY2
			2.R3.CY3
		'Quick' static tension test 15/11/98	2.R3.T4
		Tension failure 20/04/99	3.R3.T5
R4	As above	Reaction for GOPAL pile tests 01/11 to 06/11/98	–
Tip at	Driven 24/08/98	Tension to 2MN—no failure 16/11/98	2.R4.T1
19.37 m		Cyclic tension test 17/11/98	2.R4.CY2
		'Quick' tension to failure 17/04/99	2.R4.T3
		Cyclic tension test 18/11/98	2.R4.CY4
		Tension failure 18/11/98	2.R4.T5
		Extended 1000 cycle tension test—no failure 23/04/99	3.R4.CY6
		'Quick' tension to failure 24/04/99	3.R4.T7
R5	As above	Reaction for GOPAL pile tests 29/10 to 06/11/98	–
Tip at	Driven 25/08/98	Tension to 2.0MN – no failure 19/11/98	2.R5.T1
19.05m		Two sets cyclic tension tests 20 to 21/11/98	2.R5.CY2
			2.R5.CY3
		'Quick' tension test 21/11/98	2.R5.T4
		Tension failure 15/04/99	3.R5.T5
R6	As above	Reaction for GOPAL pile tests 29/10 to 30/10/98	–
Tip at	Driven 21/08/98	Tension failure 9/11/98	2.R6.T1
18.90 m		Cyclic tension test 10/11/98	2.R6.CY2
		Tension failure 11/11/98	2.R6.T3
		Cyclic tension test 12/11/98	2.R6.CY4
		'Quick' tension failure 12/11/98	2.R6.T5
		Cyclic tension failure 22/04/99	3.R6.CY6
		'Quick' tension failure 22/04/99	3.R6.T7
C1	As above	GOPAL compression failure 01/11/98	2.C1.C1
Tip at	Driven 25/08/98	Tension failure 02/11/98	2.C1.T2
10.02 m		Three sets two-way cyclic tests 02 to 05/11/98	2.C1.CY3
			2.C1.CY4
			2.C1.CY5
		Tension failure 06/11/98	2.C1.T6

where Δr is the pile peak-to-trough shaft surface roughness, and G is the operational secant shear stiffness. Jardine et al. (2005b) provide simple rules to estimate G, and the base resistance q_b from CPT tests. Variations between the predicted individual capacities and the overall mean predicted capacity of the reaction piles of up to 17.1% are indicated in Table 2, falling within the standard deviation expected from the database studies. The results from the static tests also correlate with the hierarchy of driving resistances reported by Jardine et al. (2006).

Fig. 7 reproduces the latter authors' summary of tension shaft capacities, normalised by the respective ICP design capacity predictions, and corrected for the pile and soil plug weights. It is shown that the capacities of piles C1, R1 and R2 varied with age after driving. Undisturbed piles showed marked and steady gains with time (defined by the Intact Ageing Characteristic, IAC), while pre-failed piles followed discontinuous trends. Testing to failure generally reduced capacity. Some recovery took place afterwards, but this could not match the gains developed by undisturbed piles. Static testing to failure before any particular cyclic experiment could degrade capacity, and piles tested after high-level cyclic testing generally could not achieve their pre-cycling capacities. A mixed series of first-time tests and re-tests was staged to allow best estimates to be made of the static tension capacities applying before each cyclic loading test, accounting for local variations, possible brittleness and ageing. These estimates are listed in Table 3.

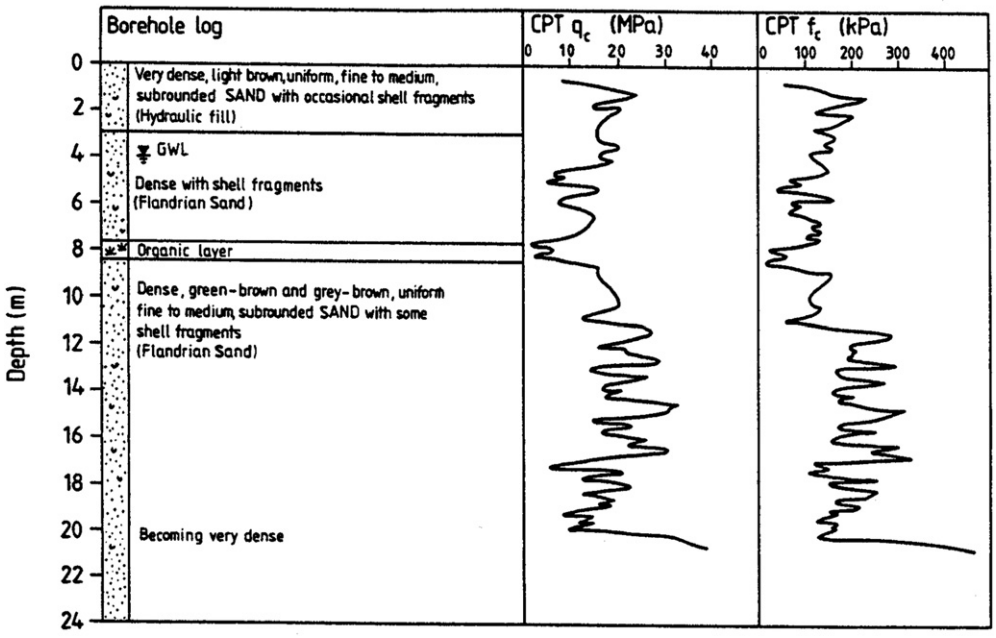

Fig. 4. Typical geotechnical profiles for CLAROM/Imperial College test site (Chow, 1997).

1.5. Pile testing procedures

Precision monitoring and control (PMC) of Teeside (UK) provided specialist pile testing equipment and site personnel. Loads were controlled by an automated hydraulic system and the beam arrangements described by Jardine et al. (2006). A high quality load cell was employed and four independent displacement transducers were attached to reference beams supported at least 2 m away from the piles and reaction pads. Screens erected over the installations reduced thermal and environmental effects. Loading was controlled by a regulator that could cycle (with periods between 1 and 2 min, depending on pile response), between maxima and minima that could generally be maintained to ± 5 kN over extended durations. Figs. 8 and 9 illustrate a typical one-way test, 2.R3.CY3, that failed after around 15 cycles. The waveforms were intended to be sinusoidal, but compliance effects led to time histories that were less rounded and symmetrical than sine waves.

'Slow' and 'quick' static tests were staged to track shaft capacity; Jardine et al., (2006). 'Slow' tests were governed by creep rate criteria and involved incremental loading stages separated by pauses and could take many hours, while 'quick' tests led to failure within tens of minutes. Check tests indicated that capacity did not vary significantly with loading rate, although 'quick' tests developed smaller displacements. Some brittle tension failures were noted while others exhibited stick-slip modes. Jardine and Standing (2000) reported load-displacement curves for all tests, noting that all tension failures required displacements less than 7% of the pile diameter while the compression test on C1 developed no distinct peak. Static tests were generally unloaded as soon as failure was clear, so limiting the damage to capacity.

2. Cyclic test results and interpretation

This study's main focus is on cyclic failure characteristics and Table 3 summarises the loads applied (note that load values are expressed to nearest 5 kN). One aim was to identify piles that were subjected to stable, unstable or meta-stable cycles as defined below.

- Stable (S): pile head displacements accumulate slowly over hundreds of cycles, under one-way loading (with either tension or compressions loads applied) or two-way loading (involving tension followed by compression loads applied, or vice versa, passing through zero load during each cycle).
- Unstable (US): displacements develop rapidly under one-way or two-way conditions leading to failure at $N < 100$ and marked shaft capacity losses.
- Metastable (MS): pile head displacements accumulate at moderate rates over tens to hundreds of cycles without stabilising and cyclic failure develops within the $100 < N < 1000$ range.

Stable cycles lead to shaft capacity gains, while either increases or decreases in shaft capacity are possible with metastable cycles. Cyclic failure was identified as: (i) accumulated displacements reaching 10% of the pile diameter (45.7 mm), or (ii) a sudden acceleration in permanent displacement rates. Rates were considered *slow* if < 1 mm/10^3

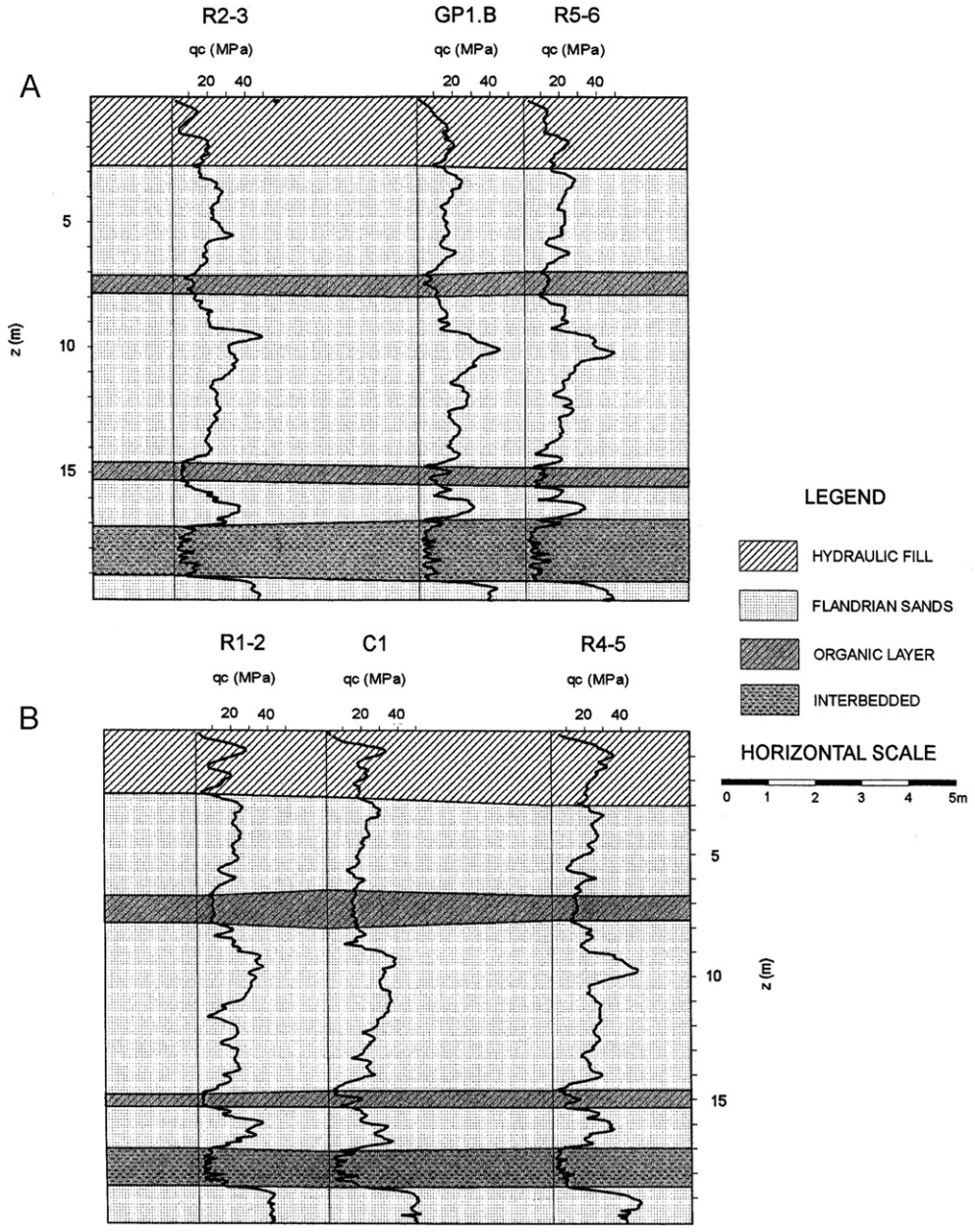

Fig. 5. CPT profiles with depth and interpreted soil profile (see Fig. 3 for locations of Sections A-A and B-B).

cycles (10 times the limit applied by Tsuha et al. to their 36 mm Mini-ICP pile tests).

Table 4 lists the cyclic test outcomes. Applying the above definitions, the cycles applied led to just one example of a stable test, while nine were unstable and four metastable. We describe and discuss examples of each below. Jardine and Standing (2000) reported equivalent plots for all 14 cyclic tests.

2.1. Stable cyclic loading

Figs. 10 and 11 illustrate results from the stable cycle test: 3.R4.CY6. A slender and immobile load-displacement loop was set up after the first cycle. The permanent displacements grew by just 0.4 mm over the first 500 cycles of one-way tension cycling (from 0 to 800 kN) but then stabilised, or even reduced, as N increased to 1000. Cyclic amplitudes also tended to reduce slightly once $N > 500$. The subsequent quick static loading test (3.R4.T7) showed an 18% (albeit brittle) gain over the estimated pre-cycling tension capacity.

2.2. Metastable cyclic loading

Metastable cyclic behaviour is illustrated in Figs. 12 and 13 using results from test 3.R6.CY6, where the pile eventually failed under metastable cycling (similar to 2.R5.CY2). Permanent displacement rates grew steadily

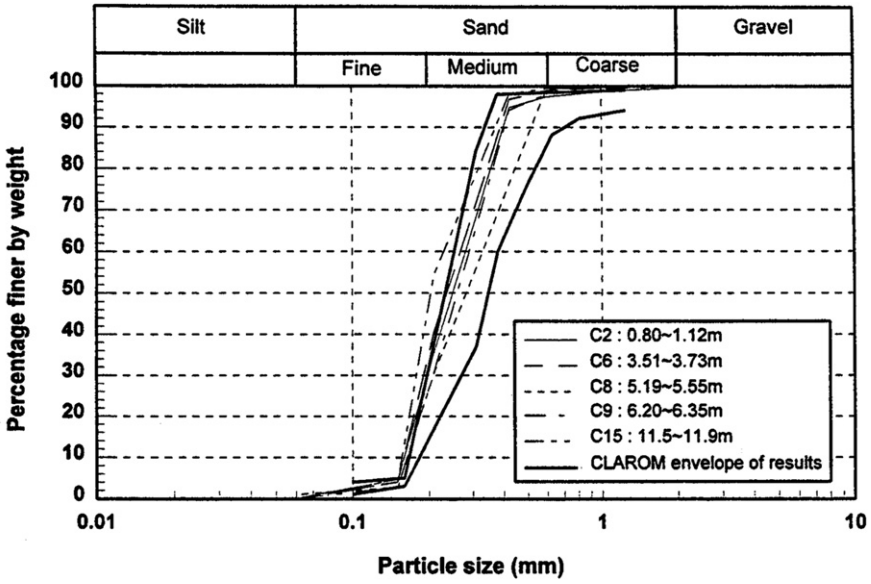

Fig. 6. Range of particle size distribution curves from CLAROM borehole (Chow, 1997).

Table 2
ICP design assessment of pile capacity at nominal 10-day age.

Pile	CPT profile applied	Calculated ICP design capacity (kN)
R1	R1–R2	1500 tension (3.3% above mean for reaction piles)
R2	Mean of R1–R2 and R2–R3	1390 tension (4.3% below mean for reaction piles)
R3	R2–R3	1430 tension (1.5% below mean for reaction piles)
R4	R4–R5	1700 tension (17.1% above mean for reaction piles)
R5	Mean of R4–R5 and R5–R6	1420 tension (2.2% below mean for reaction piles)
R6	R5–R6	1270 tension (12.5% below mean for reaction piles)
C1	C1	910 (shaft: compression), 673 (shaft: tension), 753 (base)

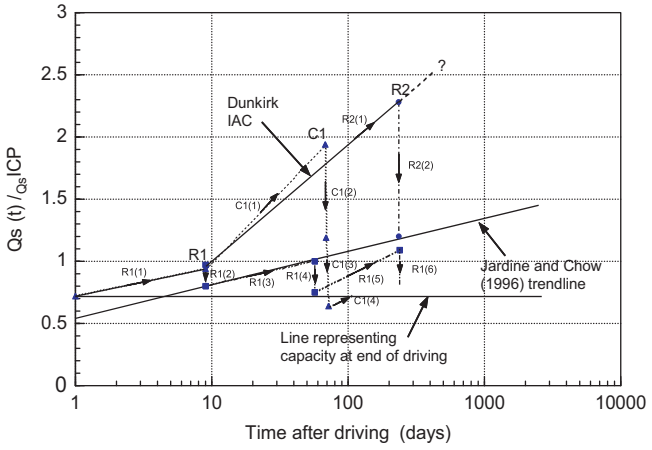

Fig. 7. Normalised pile capacities versus time for first-time and pre-failed tension tests for control pile C1 and reaction piles R1 and R2 (Jardine et al., 2006).

by an order of magnitude from about 0.013mm/cycle (up to $N=50$) up to about the 190th cycle, after which rates accelerated more sharply. The pile pulled out by 8 mm over its last cycle, with stick-slip fluctuations between 1200 and 1400 kN. Tension loads varied between 1150 and 1600 kN (about a similar mean) in a quick test, 3.R6.T7. Overall, the cyclic and static capacities fell 14 to 21% below the estimated pre-cycling tension capacity. Cyclic failure loads generally matched the tension capacities seen in subsequent tension tests, indicating that rate effects and capacity losses due to unloading after cyclic failure are either negligible or self cancelling. All four metastable cycle tests involved significant tension capacity reductions; see Table 3.

2.3. Unstable cyclic loading

The behaviour of an exemplar unstable one-way high-level cyclic test, 2.R3.CY3, was illustrated earlier in Figs. 8 and 9. The load-displacement data are added in Fig. 14. While almost constant displacement amplitudes (± 3.1 mm) developed over the first $N=13$ cycles, the permanent displacements were initially relatively high (around 0.5 mm per cycle) and accelerated progressively after reaching $N=7$. The test was terminated after displacing 10% of the pile diameter (i.e. 46 mm). The pile was unable to re-achieve its target of 1900 kN tension on re-loading from the 13th cycle

Table 3
Key features of static and cyclic tension tests.

Test code	Key observations
1.R1.T1	Ductile failure: 1450 kN (24 mm displacement)
2.R1.T2	Marginally brittle failure: 1500 kN (8 mm displacement)
3.R1.T3	Marginally brittle failure: 1645 kN (8 mm displacement)
3.R2.T1	Ductile failure: 3210 kN (34 mm displacement)
3.R2.CY2	$Q_{cyclic}=1000$ kN, $Q_{mean}=1000$ kN; estimated initial $Q_{max}=2500$ kN
3.R2.T3	'Stick-slip' failure: 1655 kN
2.R3.T1	No failure on loading to 2000 kN (10.3 mm displacement)
2.R3.CY2	$Q_{cyclic}=700$ kN, $Q_{mean}=700$ kN; estimated initial $Q_{max}=2315$ kN
2.R3.CY3	$Q_{cyclic}=950$ kN, $Q_{mean}=950$ kN; estimated initial $Q_{max}=2050$ kN
2.R3.T4	'Stick-slip' failure: 1650 kN in 'quick' test
3.R3.T5	Brittle 'stick-slip' failure: 1990 kN (10 mm displacement)
2.R4.T1	No failure on loading to 2000 kN (8.7 mm displacement)
2.R4.CY2	$Q_{cyclic}=1000$ kN, $Q_{mean}=1000$ kN; estimated initial $Q_{max}=2960$ kN
2.R4.T3	Failure: 2000 kN in 'quick' test
2.R4.CY3	$Q_{cyclic}=750$ kN, $Q_{mean}=1250$ kN; estimated initial $Q_{max}=2100$ kN
2.R4.T5	Brittle 'stick-slip' failure: 2000 kN, reducing to 1450 kN
3.R4.CY6	$Q_{cyclic}=400$ kN, $Q_{mean}=405$ kN; estimated initial $Q_{max}=2110$ kN
3.R4.T7	Brittle 'stick-slip' failure: 2490 kN (reducing to 1900 kN) in 'quick' test
2.R5.T1	Loaded to 2000 kN with 8.9 mm displacement; estimated Capacity=2450 kN
2.R5.CY2	$Q_{cyclic}=750$ kN, $Q_{mean}=1250$ kN; estimated $Q_{max}=2465$ kN
2.R5.CY3	$Q_{cyclic}=700$ kN, $Q_{mean}=700$ kN; estimated $Q_{max}=2000$ kN
2.R5.T4	'Stick-slip' failure: average 1300 kN in 'quick' test
3.R5.T5	Brittle failure: 1795 kN (reducing to 1636 kN)
2.R6.T1	Loaded to 2400 kN with 30 mm displacement, estimated Capacity=2450 kN
2.R6.CY2	$Q_{cyclic}=750$ kN, $Q_{mean}=1250$ kN; estimated $Q_{max}=2000$ kN (test aborted after first cycle)
2.R6.T3	Ductile failure: 1585 kN (7 mm displacement)
2.R6.CY4	$Q_{cyclic}=700$ kN, $Q_{mean}=700$ kN; estimated $Q_{max}=1585$ kN
2.R6.T5	'Stick-slip' failure: average 1325 kN in 'quick' test
3.R6.CY6	$Q_{cyclic}=700$ kN, $Q_{mean}=700$ kN; estimated $Q_{max}=1650$ kN
3.R6.T7	'Stick-slip' failure: 1425 kN
2.C1.C1	Compression load to 2820 kN after 34 mm, load at 46 mm estimated=2850 kN
2.C1.T2	'Stick-slip' tension: 820 kN (33 mm displacement)
2.C1.CY3	$Q_{cyclic}=600$ kN, $Q_{mean}=-40$ kN (compression); amplitudes increase suddenly at $N=21$ after correct loading applied at $N=17$ with equal tension and compression loads of 600 kN and pile reverses to pull out 45 mm in next 20 cycles, estimated initial $Q_{max}=840$ kN
2.C1.CY4	$Q_{cyclic}=445$ kN, $Q_{mean}=165$ kN (tension); large permanent displacement with each cycle; pile pulls out 45 mm in 3 cycles, estimated initial $Q_{max}=620$ kN
2.C1.CY5	$Q_{cyclic}=410$ kN, $Q_{mean}=10$ kN (tension); amplitudes increase suddenly at $N=2$ and pile reverses to pull out 45 mm in next 10 cycles, estimated initial $Q_{max}=620$ kN
2.C1.T6	'Stick-slip' failure, maximum load of 500 kN at 46 mm

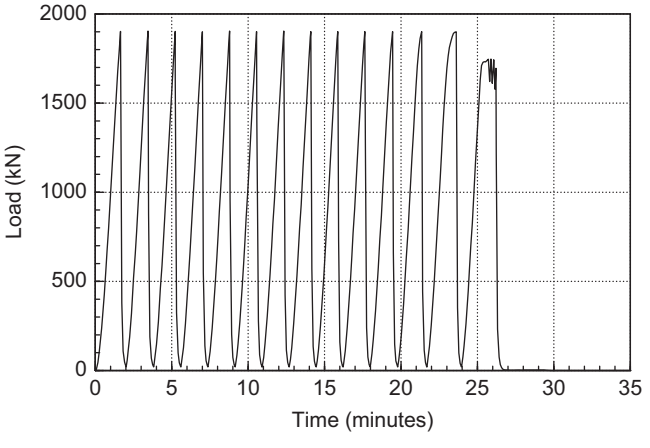

Fig. 8. Tension loads applied in typical unstable tension cycle test: 2.R3.CY3.

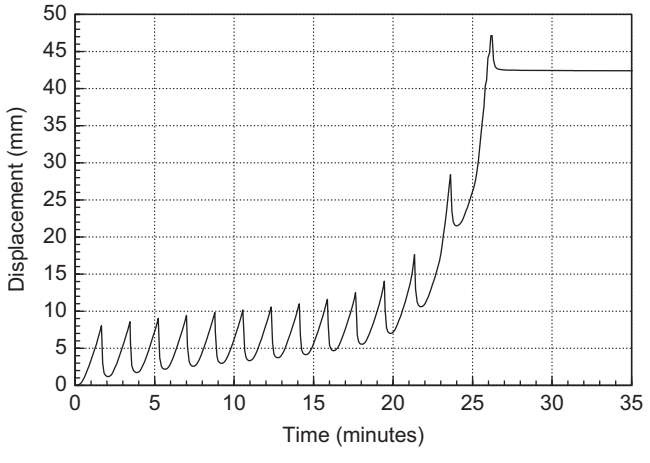

Fig. 9. Upward pile head displacements developed over 14 cycles in typical unstable tension cycle test: 2.R3.CY3.

Table 4
Outcomes of all cyclic loading tests.

Test	Key factors	Class
3.R2.CY2	$Q_{cyclic}/Q_{max}=0.40$, $Q_{mean}/Q_{max}=0.40$. Failed in 9 cycles. Initial permanent displacement rate 0.3 mm/cycle; 9 mm over last cycle	US
2.R3.CY2	$Q_{cyclic}/Q_{max}=0.30$, $Q_{mean}/Q_{max}=0.30$. Unfailed after 200 cycles. Permanent displacement rate constant at 3.5 mm/10^2 cycles	MS
2.R3.CY3	$Q_{cyclic}/Q_{max}=0.46$, $Q_{mean}/Q_{max}=0.46$. Brittle failure after 12 cycles. Initial permanent displacement rate 0.5 mm/cycle; 21 mm over last cycle	US
2.R4.CY2	$Q_{cyclic}/Q_{max}=0.34$, $Q_{mean}/Q_{max}=0.34$. Unfailed after 221 cycles. Average permanent displacement rate: 8.5 mm/10^2 cycles, increasing sharply over last 30 cycles	MS
2.R4.CY4	$Q_{cyclic}/Q_{max}=0.36$, $Q_{mean}/Q_{max}=0.59$. Failed in 3 cycles. 6 mm over last cycle	US
3.R4.CY6	$Q_{cyclic}/Q_{max}=0.19$, $Q_{mean}/Q_{max}=0.19$. Unfailed after 1000 cycles. After first cycle, permanent displacement rate <1 mm/10^3 cycles	S
2.R5.CY2	$Q_{cyclic}/Q_{max}=0.30$, $Q_{mean}/Q_{max}=0.51$. Failed after 345 cycles. Average permanent displacement rate: 7.7 mm/10^2 cycles, higher at start and increasing significantly after $N=275$; 6 mm over last cycle	MS
2.R5.CY3	$Q_{cyclic}/Q_{max}=0.35$, $Q_{mean}/Q_{max}=0.35$. Failed after 27 cycles. Initial permanent displacement rate around 4.0 mm/10^2 cycles, increasing sharply after $N=21$; 8 mm over last cycle	US
2.R6.CY2	$Q_{cyclic}/Q_{max}=0.38$, $Q_{mean}/Q_{max}=0.63$. Failed in 1 cycle	US
2.R6.CY4	$Q_{cyclic}/Q_{max}=0.44$, $Q_{mean}/Q_{max}=0.44$. Failed after 24 cycles. Initial permanent displacement rate around 3.5 mm/10^2 cycles, increasing sharply at $N=17$; 9 mm over last cycle	US
3.R6.CY6	$Q_{cyclic}/Q_{max}=0.42$, $Q_{mean}/Q_{max}=0.42$. Failed after 206 cycles. Average permanent displacement rate: 4.6 mm/10^2 cycles, increasing markedly after $N=190$; 8 mm over last cycle	US
2.C1.CY3	$Q_{cyclic}/Q_{max}=0.71$, $Q_{mean}/Q_{max}=-0.05$. Failed after 40 cycles. Initially tending to settle, changing sign of permanent displacement rate at $N=21$, finally pulling out; 5 mm over last cycle	US
2.C1.CY4	$Q_{cyclic}/Q_{max}=0.72$, $Q_{mean}/Q_{max}=0.27$. Failed in two cycles. Pulling out 83 mm overall in 5 cycles	US
2.C1.CY5	$Q_{cyclic}/Q_{max}=0.68$, $Q_{mean}/Q_{max}=0.02$. Failed after 8 cycles. Rapidly increasing permanent displacement rate and amplitudes over final stages; pulling out 8 mm over last (13th) cycle	US

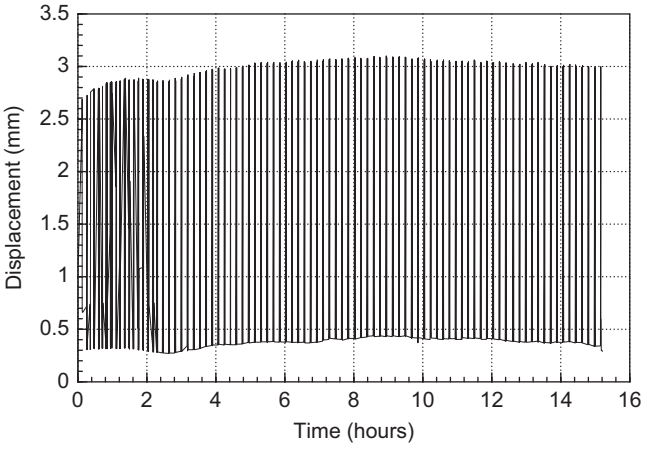

Fig. 10. Displacement-times trace over 1000 cycles for stable tension cycle test: 3.R4.CY6. (roughly only every tenth cycle shown).

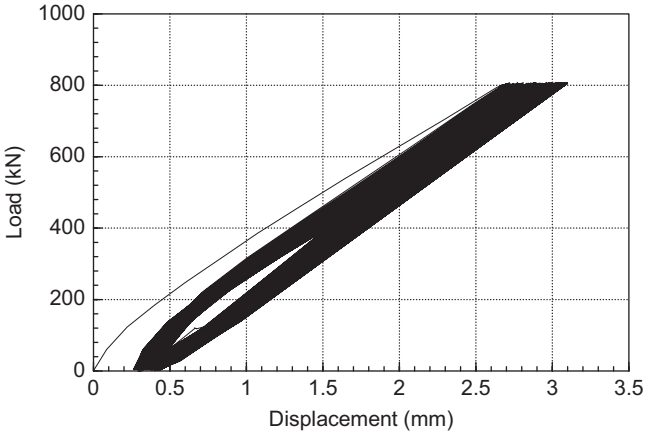

Fig. 11. Load-displacement curves over 1000 cycles for stable tension cycle test: 3.R4.CY6.

and lost about 10% of its capacity in its final brittle failure. An overall capacity loss of 24% is interpreted.

The two-way high-level cyclic experiment 2.C1.CY3 was the first cyclic test and one of the most difficult to perform. As illustrated in Figs. 15 to 17, the first 16 cycles inadvertently applied 100 kN less tension than intended; the loading system also halted unintentionally at $N=20$ for 25 min and the loading system had to be re-adjusted. Despite these imperfections, 2.C1.CY3 is the most interesting two-way test. Its early tendency to settle (at an initial rate of 0.50 mm/cycles) corresponds to the maximum compressive loads applied being greater than the tensile maximum (-600 kN compression versus 500 kN tension). This trend continued up to the time when the loads were adjusted to give equal increments of tension and compression load maxima from $N=17$. From this point the displacement amplitudes increased sharply. The resumed balanced cycling imposed after $N=21$ led to progressively increasing upward pile head displacements. Failure occurred after 20 further cycles of growing amplitudes and uplift drift. The post-cycling tension capacity (620 kN) was close to the maximum cyclic tension. The overall tension capacity loss is estimated as 26–29%.

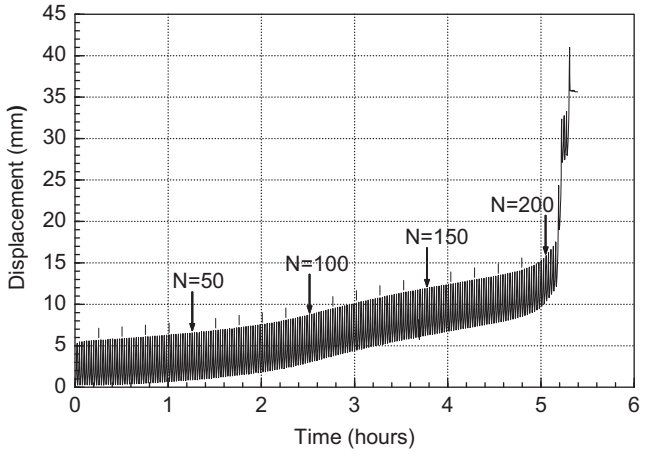

Fig. 12. Displacement-time trace over 208 cycles for typical metastable tension cycle test 3.R6.CY6.

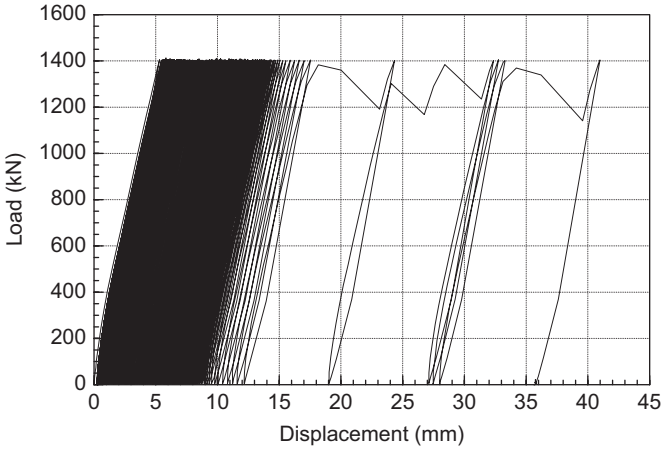

Fig. 13. Load-displacement curves over 208 cycles for typical metastable tension cycle test 3.R6.CY6.

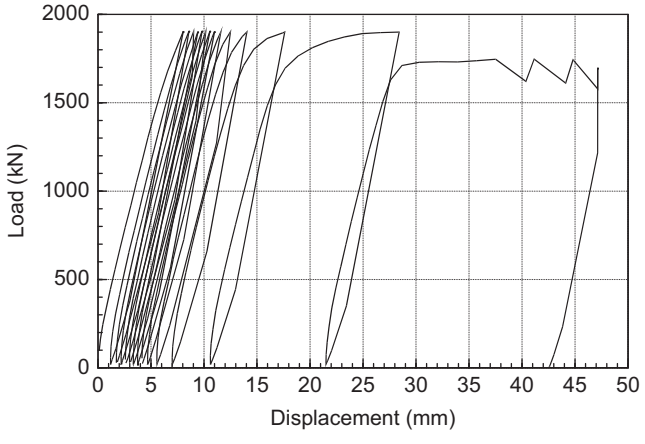

Fig. 14. Load-displacement curves over 41 cycles for typical unstable tension cycle test 2.R3.CY3.

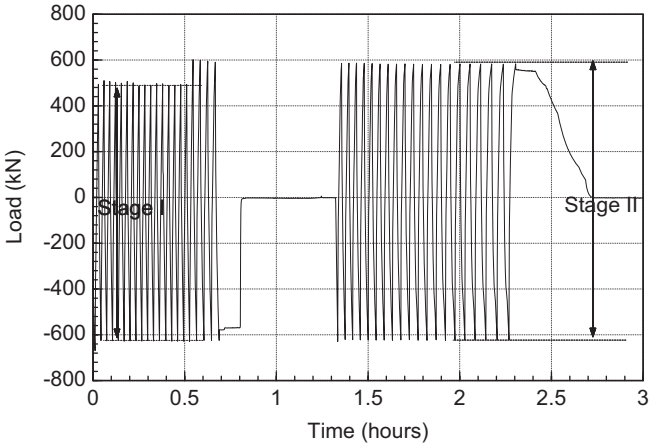

Fig. 15. Load-time trace over 41 cycles for two-way unstable cycle test 2.C1.CY3.

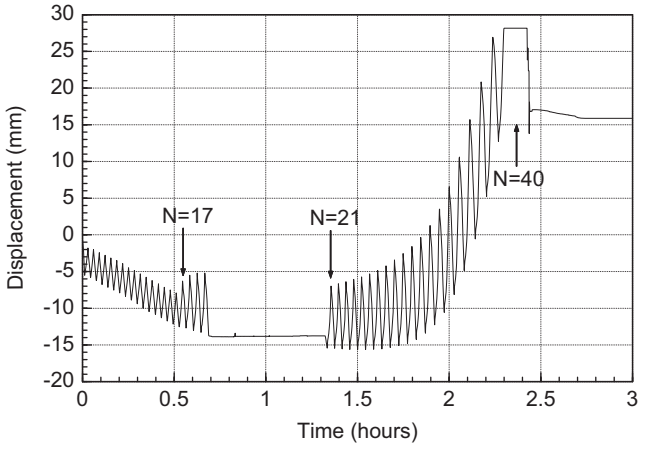

Fig. 16. Displacement-time trace over 40 cycles for two-way unstable cycle test 2.C1.CY3.

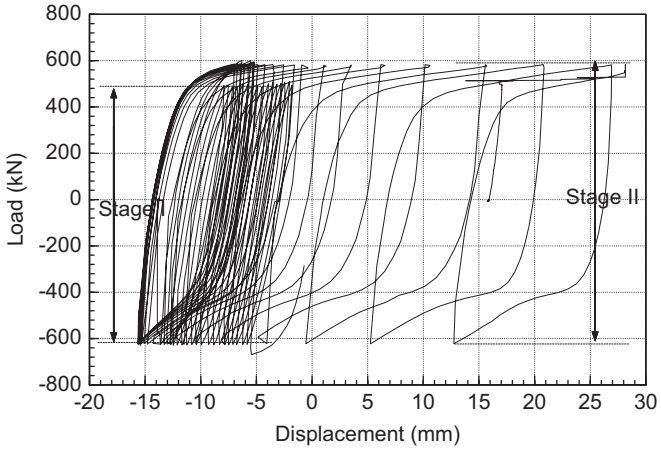

Fig. 17. Load-displacement curves over 40 cycles for two-way unstable cycle test 2.C1.CY3.

2.4. Cyclic displacement trends and predictions

Many of the tests showed cyclic displacement amplitudes that remained relatively steady until failure was approached. As described by Jardine et al. (2005a), multiple numerical analyses were made of the Dunkerque pile tests with the Imperial College Finite Element Program, ICFEP (Potts and Zdravkovic, 1999, 2001) that utilised the detailed site characterisation data referred to in the introduction. While no attempt was made to match the field rates of permanent displacement or capacity reductions, the ICFEP analyses provided a generally good match for the field static load test capacities and the load-displacement responses; see Jardine et al. (2005a). They also reproduced the initial field stiffness responses to load cycling, confirming that the first loops fitted the patterns expected for the non-linear, anisotropic, pressure dependent, Dunkerque sand. The ICFEP analyses provided further insights into the local distributions of shear stresses acting over the shafts. For example, applying a purely tension cycle applied at the pile head induced two-way cycling failure (i.e. alternating between upward and downward shaft shear stresses and relative slip) at the top of the shaft that extended down to a depth that depended on the applied loading level. Similar observations have been reported by Jardine (1991, 1994). The analyses also established the conditions that would promote progressive top-down degradation, with the two-way cycling zone (and the full mobilisation of tension shaft resistance) migrating downwards with each cycle under unstable cyclic loading.

While the loading patterns that led rapidly to cyclic failure also tend to show relatively high initial rates of cyclic displacement, the field tests did not indicate a simple link between rates of permanent displacement and the number of cycles to failure; see Table 4. Further analysis of these data is in hand; Tsuha et al. (2012) argue that the permanent displacement and capacity reduction trends depend on the complexities of relatively small-strain kinematic yielding, dilatancy in the soil mass and local grain crushing under interface shear.

2.5. Combined interactive cyclic failure criteria

Interaction diagrams express how the number of cycles N and the normalised loading parameters $Q_{cyclic}/Q_{max\ static}$ and $Q_{mean}/Q_{max\ static}$ act together to determine the response to uniform load cycling. Figs. 18 and 19 summarise these interactions for the Dunkerque tests. The first plot reproduces the linear interpretation made by Jardine and Standing (2000) of the combinations of cyclic and mean shaft loads required to bring about cyclic shaft failure in specified numbers (N_f) of regular cycles. With this are shown the positions of N_f lines obtained by applying the Jardine et al. (2005b) predictive approach set out in Appendix A as calibrated for conditions at Dunkerque. The latter model involves fitting the empirical parameters A, B and C to either pile load tests or cyclic laboratory (simple shear, triaxial or hollow cylinder) experiments. The Dunkerque model was derived from laboratory constant volume simple shear tests on a comparable North Sea dense sand. Atkins (2000) reports how the approach outlined in Appendix A was extended successfully into more complex numerical post-predictions (Class C after Lambe, 1973) of the Dunkerque cyclic tests. The predicted numbers of cycles to failure, N_f, are broadly consistent with the Dunkerque field tests, although individual tests could deviate from interpreted lines significantly. Precise predictions are hard to obtain (see Figs. 18 and 19).

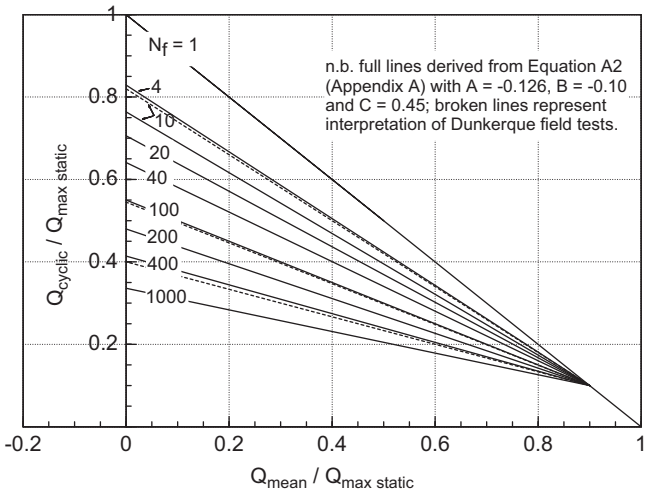

Fig. 18. Interaction diagram based on simplified methodology given in Appendix A and field test interpretation for predicting number of cycles to failure N_f in terms of normalised loading parameters Q_{cyclic}/Q_{max} and Q_{mean}/Q_{max}.

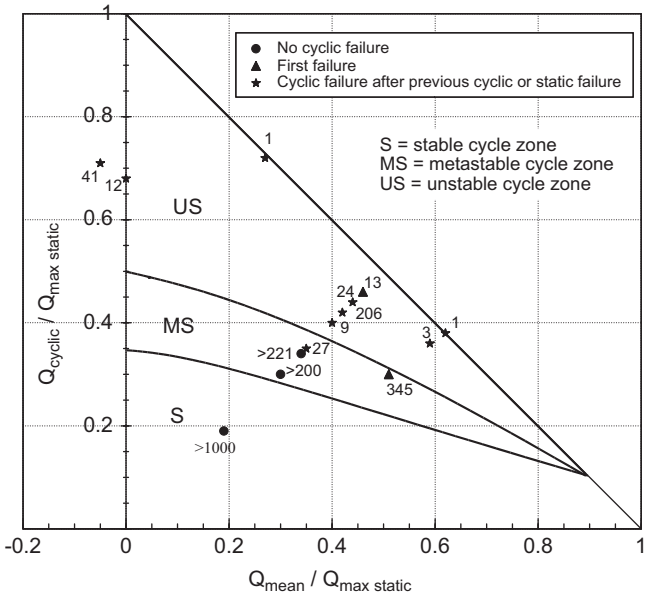

Fig. 19. Interaction diagram indicating influence of number of cycles N and normalised loading parameters Q_{cyclic}/Q_{max} and Q_{mean}/Q_{max} on cyclic response along with tentative stable, metastable and unstable cycle zones.

Fig. 19 extends the interpretation by proposing boundaries for the stable, metastable and unstable cyclic zones of behaviour. The individual tests are also plotted and all but two tests conform to the proposed stable (S), unstable (US) and metastable (MS) cycle response zones. The boundaries do not appear to be sensitive to whether the piles had experienced prior cyclic or static failure, but more comprehensive testing might identify a more significant influence.

2.6. Insights offered into fundamental processes affecting cyclic stability and degradation

Tsuha et al.'s (2012) model pile experiments with medium dense fine silica sand led to broadly similar results to the field tests, including closely comparable interaction diagrams. The highly instrumented Mini-ICP experiments offer further insights into the local effective stresses applying on pile surfaces and within the sand mass during cycling.

Stable cycle loading conditions were shown to (i) avoid, over most of the shaft, local interface slip and (ii) generate effective stress paths to the adjacent soil mass that remain principally within the 'Y_2' threshold kinematic yield surface, as defined by Jardine et al. (2001), or Kuwano and Jardine (2007). Behaviour could be locally inelastic at the interface, but there was no large-scale tendency for radial contraction. Modest top-down progressive degradation might develop, but this was balanced by capacity growth elsewhere. Overall, shaft capacity increased by up to 20% as an optimised soil fabric developed.

Unstable cycle loading conditions invoked markedly inelastic behaviour. The soil mass contracted and lost mean effective stress, and local slip developed progressively as σ'_r reductions took place at the interface where a compacted and fractured shear zone grew in thickness. Shaft failure took place in less than 100 cycles, governed by a Coulomb failure law that was well-predicted by interface ring shear tests. Hysteretic "butterfly-wing" effective stress paths were observed on the shaft along with progressive top-down failure. Displacements could gradually accelerate (as in 2.R3.CY2) or reverse under two-way loading, as in 2.C1.CY2. Shaft capacities degraded markedly and failure took place with $N < 100$.

Metastable cycle loading led to an intermediate pattern. Interface slip, hysteretic stress paths, mean stress state migration and shaft capacity reductions could all develop, depending on the cyclic loading levels imposed. However, hundreds of cycles could be sustained before failure, and markedly plastic (post Y_2) behaviour was concentrated close to the shaft. It is interesting that the metastable model tests could develop either modest capacity losses or gains, depending on the severity of cycling.

Any advanced numerical modelling performed to match the above features would require constitutive models capable of capturing the cyclic soil element response, including the growth of permanent displacements, local radial effective stress and shaft capacity changes. The simplified procedures set out in Appendix A apply laboratory based constant normal stiffness or constant volume cyclic shear test data to predict the effects on capacity.

3. Summary and conclusions

Multiple static and cyclic loading experiments have been performed on large open-ended steel pipe piles driven in dense silica Dunkerque marine sand. The results have been interpreted with reference to: the comprehensive site characterisation; numerical analyses; simplified design procedures and related highly instrumented model pile experiments. Twelve main conclusions follow.

1. The piles developed substantial increases in tension resistance with time. However, aged piles lost shaft capacity on unloading after brittle first time failures.
2. Capacity recovered partially with time after cyclic or static failure, but at relatively modest rates, leading to discontinuous time-capacity traces.
3. Cyclic loading led to stable, metastable or unstable responses, depending on the loading levels normalised by the current tension capacities: $Q_{cyclic}/Q_{max\ static}$, and $Q_{mean}/Q_{max\ static}$.
4. High-level cycling under one-way and two-way conditions invoked quite different responses. The latter gave scope for higher normalised cyclic loading levels that promoted more severe cyclic losses, while the former led to less symmetric and a more progressive style of degradation.
5. Interaction diagrams express how the cyclic loading parameters N, $Q_{cyclic}/Q_{max\ static}$, and $Q_{mean}/Q_{max\ static}$ affect cyclic response. The diagram interpreted for Dunkerque captured key aspects of the 14 tests performed and has a similar pattern to the model tests reported by Tsuha et al. (2012).
6. The simplified procedures outlined by Jardine et al. (2005b) provide a good quantification scheme for modelling and predicting the effects of cycling on shaft capacity.
7. Low-level cycling can have beneficial effects on pile capacity, and piles can self-heal with time after modest losses of cyclic capacity. Tension capacity gains of up to $\sim$20% have been developed after applying stable cyclic loading to piles in field and model tests.
8. High-level cyclic loading can impact very significantly on shaft capacity.
9. Associated numerical studies and instrumented model pile tests show that stable cyclic loading conditions avoid interface slip over most of the shaft length, and keep the soil stress paths primarily within the 'Y_2' threshold kinematic yield surface. Any modest degradation developed over the upper shaft is balanced by capacity growth elsewhere.
10. The same studies show that unstable cyclic loading conditions invoke markedly inelastic behaviour in the

sand and at the shaft-sand interface, leading to local slip (governed by a Coulomb law) and soil contraction from the first cycle. Top-down progressive failure develops; displacements can accelerate monotonically in one-way tests or reverse under two-way loading. Failure occurs within 100 cycles and shaft capacity degrades strongly.

11. Metastable cyclic loading leads to an intermediate mechanical response at the pile-soil interface. Interface slip, hysteretic stress paths, mean stress state migration and shaft capacity reductions could all develop, depending on the cyclic loading levels imposed. While piles could sustain hundreds of metastable cycles without failing, significant capacity losses were noted in all four of the metastable cyclic loading Dunkerque field tests.
12. Cyclic loading can degrade pile capacity and stiffness markedly and its effects should both be researched further and addressed more routinely when designing foundations that carry a high proportion of variable environmental loading.

Acknowledgements

The Authors acknowledge funding from the UK Health and Safety Executive (HSE) and the EU and thank the Port Autonome de Dunkerque for providing the site. They also acknowledge the contributions of Mr Eric Parker of D'Appolonia (Italy); Precision Monitoring and Control (UK); Dr Nebojsa Kovacevic of GCG (UK); former colleagues at Imperial College, Dr Fiona Chow, Dr Reiko Kuwano and Mr Tim Connolly; the UK Building Research Establishment's in-situ testing team and Simecsol of Dunkerque, France.

APPENDIX A. Simplified procedure for predicting cyclic interaction diagram for shaft capacity degradation of Dunkerque piles under cyclic loading

The analysis flows from Eq. (A1) as given by Jardine et al. (2005b) that expresses the changes expected in local radial effective stress acting on the pile shaft due to cyclic loading.

$$\Delta\sigma_r'/\sigma_{rc}' = A\left(B+\tau_{cyclic}/\tau_{max\ static}\right)N^C \quad (A1)$$

Jardine et al. (2005b) note that a variant of adopting $\log N$ in place of the N^C term may be more applicable in some cases. Cyclic soil element, model or field tests can be conducted to choose the most appropriate variant and parameters.

The key assumptions and steps applied for the Dunkerque piles are as follows.

1. The entire applied cyclic load is taken in shaft resistance, with base cyclic loading being negligible. This assumption is marginally conservative in cases where some of the loading is compressive.
2. We can neglect the effect of constrained interface dilation on shaft capacity. The ICP approach predicts that pile loading will engender such a component of radial effective stress change that is inversely related to pile radius. While this contribution can be significant for small piles, it is relatively minor ($<15\%$) for the industrial-scale Dunkerque piles. Naturally, the analysis can be extended to cover interface dilation in cases where this is important.
3. Neglecting interface dilation leads to local shaft pile capacity being given by $\tau_f=\sigma'_{rf}\tan\delta$ and the change in tension capacity can be calculated from the changes σ'_r given by Eq. (A1) as linear functions of $\tau_{cyclic}/\tau_{max\ static}$. Noting that at failure $\tau_f=\tau_{cyclic}+\tau_{mean}$ the combinations of $\tau_{cyclic}/\tau_{max\ static}$ and $\tau_{mean}/\tau_{max\ static}$ required to reach failure under cycling can be expressed in an interaction diagram as a family straight lines, each representing a constant N_f (where N_f is the number of cycles to failure).
4. We assume for the Dunkerque tests that the local Eq. (A1) can be applied globally to cover the average degradation of shaft resistance, and hence overall shaft capacity. The expression for $\Delta Q_{static\ shaft\ resistance}=\Delta Q_{max\ static}$ the loss of static shaft resistance compared with its original pre-cycling value is then

$$\Delta Q_{max\ static}/Q_{max\ static} = A\left(B+Q_{cyclic}/Q_{max\ static}\right)N^C \quad (A2)$$

5. Direct calibration with the Dunkerque test results gives the following values:

$$A=-0.126,\ B=-0.10,\ C=0.45$$

6. These values reproduce the Dunkerque lines of constant N_f well, as shown on Fig. 18.
7. A further limit is assumed to apply to the levels of $Q_{cyclic}/Q_{max\ static}$ below which cycling improves rather than degrades capacity. The single stable one-way test at Dunkerque showed that this applied for cycling with

$$Q_{cyclic}/Q_{max\ static} = Q_{average}/Q_{max\ static} = 0.25$$

8. Lower limits will apply at higher values of $Q_{average}/Q_{max\ static}$ and possibly higher limits at lower average load ratios. A suggestion is given on Fig. 19 as to the shape of the curves that separate stable and metastable states.
9. The effects of non-uniform batches of cycles that exceed the stable zone limits can be considered through a 'moving equivalent cycle' approach in which the cycles are grouped into batches of cycles with constant amplitudes.
10. Consider the case where a first series of N_i cycles is applied at cyclic load level $(Q_{cyclic}/Q_{max\ static})_i$ before moving to the next $(i+1)$th batch involving N_{i+1} cycles applied at load level $(Q_{cyclic}/Q_{max\ static})_{i+1}$.

11. The equivalent number of cycles $N_{\text{Equivalent}}$ that would need to have been applied at the $i+1$ level to produce the same degree of degradation as that developed in the preceding (ith) set is calculated as

$$\Delta Q_{\text{max static}}/Q_{\text{max static}} = A\left(B+\left(Q_{\text{cyclic}}/Q_{\text{max static}}\right)_i\right)N_i^C = A\left(B+\left(Q_{\text{cyclic}}/Q_{\text{max static}}\right)_{i+1}\right)N_{\text{Equivalent}}^C$$

so that

$$\left(B+\left(Q_{\text{cyclic}}/Q_{\text{max static}}\right)_i\right)N_i^C = \left(B+\left(Q_{\text{cyclic}}/Q_{\text{max static}}\right)_{i+1}\right)N_{\text{Equivalent}}^C$$

giving

$$N_{\text{Equivalent}} = N_i\left[\left(B+\left(Q_{\text{cyclic}}/Q_{\text{max static}}\right)_i\right) \Big/ \left(B+\left(Q_{\text{cyclic}}/Q_{\text{max static}}\right)_{i+1}\right)\right]^{1/C} \quad \text{(A3)}$$

12. The value of $N_{\text{Equivalent}}$ is updated by adding N_{i+1}, the number of cycles in batch $i+1$, to find the equivalent number of cycles at the end of batch $i+1$. The total degradation of capacity at this point is found by substituting $N_{\text{Equivalent}}$ into Eq. (A2).
13. Eq. (A3) is updated again on moving to the next $(i+2)$th batch of cycles, and the process repeated for the full set of cyclic batches.

References

Atkins Consultants Ltd., 2000. Cyclic degradation of offshore piles. HSE Offshore Technology Report OTO 2000 013. Health and Safety Executive, London.

Brucy, F., Meunier, J., Nauroy, J.F., 1991. Behaviour of pile plug in sandy soils during and after driving. In: Proceedings of the 23rd Offshore Technology Conference, OTC 6514, Houston, pp. 145–154.

Chow, F.C., 1997. Investigations Into Displacement Pile Behaviour for Offshore Foundations. Ph.D. Thesis. University of London, Imperial College.

Jardine, R.J., 1991. The Cyclic Behaviour of Offshore Piles. Chapter. In: Brown, O'Reilly (Eds.), 'The Cyclic Loading of Soils'. Blackie and Son, Glasgow.

Jardine, R.J., 1994. Offshore Pile Design For Cyclic Loading: North Sea clays. HSE Offshore Technology Report, OTN 94 157.85.

Jardine, R.J., Standing, J.R., 2000. Pile Load Testing Performed for HSE Cyclic Loading Study at Dunkirk, France. Offshore Technology Report OTO 2000 007, Health and Safety Executive, London, two volumes 60p, 200p.

Jardine, R.J., Kuwano, R., Zdravkovic, L., Thornton, C., 2001. Some fundamental aspects of the pre-failure behaviour of granular soils. In: Proceedings of the 2nd International Symposium on pre-failure. Deformation Characteristics of Geomaterials, IS-Torino, vol. 2, Swets and Zeitlinger, Lisse, pp. 1077–113.

Jardine, R.J., Standing, J.R., Kovacevic, N., 2005a. Lessons learned from full-scale observations and the practical application of advanced testing and modelling. Keynote paper. Proceedings of International Symposium on Deformation Characteristics of Geomaterials, vol. 2, Lyon, pub Balkema, Lisse, pp. 210–245.

Jardine, R.J., Chow, F.C., Overy, R., Standing, J.R., 2005b. ICP Design Methods for Driven Piles in Sands and Clays. Thomas Telford Ltd., London 105p.

Jardine, R.J., Standing, J.R., Chow, F.C., 2006. Some observations of the effects of time on the capacity of piles driven in sand. Géotechnique 56 (4), 227–244.

Kuwano, R., 1999. The Stiffness and Yielding Anisotropy of Sand. Ph.D. Thesis. University of London, Imperial College.

Kuwano, R., Jardine, R.J., 2007. A triaxial investigation of kinematic yielding in sand. Géotechnique 57 (7), 563–579.

Lambe, T.W., 1973. Predictions in geotechnical engineering. Géotechnique 23 (2), 149–202.

Lehane, B.M., 1992. Experimental Investigations of Pile Behaviour Using Instrumented Field Piles. Ph.D. Thesis. University of London, Imperial College.

Lehane, B.M., Schneider, J.A., Xu, X., 2005. A Review of Design Methods for Offshore Driven Piles in Siliceous Sand. Geomechanics Group Report GEO 05358. University of Western Australia.

Parker, E. J., Jardine, R.J., Standing, J.R., Xavier, J., 1999. Jet grouting to improve offshore pile capacity. Offshore Technology Conference, Houston, OTC 10828, Vol. 1, pp. 415–420.

Potts, D.M., Zdravkovic, L., 1999. Finite Element Analysis in Geotechnical Engineering: Theory. Pub Thomas Telford, London 440p.

Potts, D.M., Zdravkovic, L., 2001. Finite Element Analysis in Geotechnical Engineering: Application. Pub Thomas Telford, London 427p.

Tsuha, C.H.C., Foray, P.Y., Jardine, R.J., Yang, Z.X, Silva, M., Rimoy, S., 2012. Behaviour of displacement piles in sand under cyclic axial loading. Soils and Foundations 52 (3), 393–410.